AD-A170 603 BUBBLE DYNAMICS AND CAVITATION INCEPTION THEORY(U) 1/1
PENNSYLVANIA STATE UNIV UNIVERSITY PARK APPLIED
RESEARCH LAB B R PARKIN ET AL. 30 JUL 86
UNCLASSIFIED ARL/PSU/TM-86-121 N00024-85-C-6041 F/G 20/4 NL

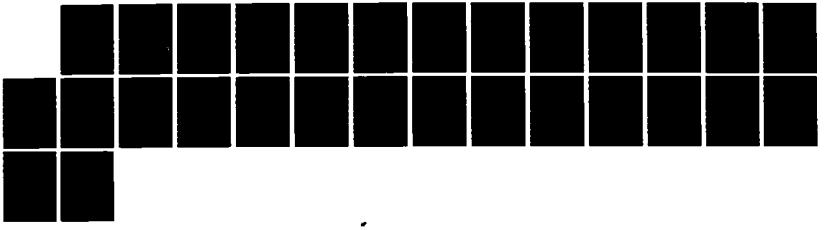

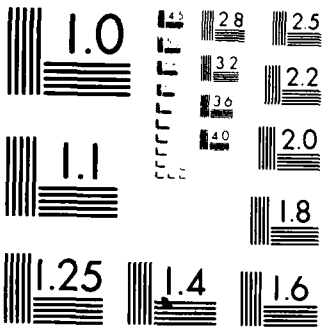

BUBBLE DYNAMICS AND CAVITATION INCEPTION THEORY

Blaine R. Parkin and Brian B. Baker

Technical Memorandum
File No. TM 86-121
30 July 1986
Contract N00024-85-C-6041

Copy No. 2

The Pennsylvania State University
Intercollege Research Programs & Facilities
APPLIED RESEARCH LABORATORY
Post Office Box 30
State College, PA 16804

NAVY DEPARTMENT

NAVAL SEA SYSTEMS COMMAND

UNCLASSIFIED

SECURITY CLASSIFICATION OF THIS PAGE (When Data Entered)

REPORT DOCUMENTATION PAGE		READ INSTRUCTIONS BEFORE COMPLETING FORM
1 REPORT NUMBER ARL/PSU TM 86-121	2. GOVT ACCESSION NO. AD-A170 603	3 RECIPIENT'S CATALOG NUMBER
4. TITLE (and Subtitle) BUBBLE DYNAMICS AND CAVITATION INCEPTION THEORY		5 TYPE OF REPORT & PERIOD COVERED Technical Memorandum 6 PERFORMING ORG. REPORT NUMBER
7 AUTHOR(s) Blaine R. Parkin and Brian B. Baker		8. CONTRACT OR GRANT NUMBER(s) N00024-85-C-6041
9 PERFORMING ORGANIZATION NAME AND ADDRESS Applied Research Laboratory Post Office Box 30 State College, PA 16804		10 PROGRAM ELEMENT, PROJECT, TASK AREA & WORK UNIT NUMBERS
11. CONTROLLING OFFICE NAME AND ADDRESS Naval Sea Systems Command [Code NSEA 63R-31] Department of the Navy Washington, DC 20362		12. REPORT DATE 30 July 1986 13. NUMBER OF PAGES 26
14 MONITORING AGENCY NAME & ADDRESS (if different from Controlling Office) David W. Taylor Naval Ship Research and Development Center [Code 1542] Department of the Navy Bethesda, MD 20084		15. SECURITY CLASS. (of this report) UNCLASSIFIED 15a. DECLASSIFICATION DOWNGRADING SCHEDULE

16. DISTRIBUTION STATEMENT (of this Report)

Approved for public release.
Distribution unlimited.
Per NAVSEA - 1 July 1986

17. DISTRIBUTION STATEMENT (of the abstract entered in Block 20, if different from Report)

18. SUPPLEMENTARY NOTES

19. KEY WORDS (Continue on reverse side if necessary and identify by block number)

bubble dynamics
cavitation inception
boundary layer separation

20 ABSTRACT (Continue on reverse side if necessary and identify by block number)

In order to provide some theoretical background and to motivate the more refined theory introduced below, we review some encouraging known theoretical results on bubble-ring cavitation inception. This review is followed by the development of the theory of bubble-ring cavitation cutoff. Its outcome, when compared with experiment, shows the need for a more refined inception theory.

DD FORM 1 JAN 73 1473 EDITION OF 1 NOV 65 IS OBSOLETE

UNCLASSIFIED

SECURITY CLASSIFICATION OF THIS PAGE (When Data Entered)

The above comparison and the basic ideas behind the cutoff theory's formulation suggest a possible approach for a refinement based on a multiple scales expansion. This seems reasonable because the forcing function pulse in "laboratory time," t, varies slowly compared to the characteristic "bubble time," τ, which characterizes the response time of a typical microscopic cavitation nucleus. The ratio of these two times gives us a small parameter, ε, appearing in the forcing function, with the result that this problem involves only a soft excitation.

Expanding the forced Rayleigh-Plesset equation and its initial conditions to the second order in ε, we find that the zeroth-order problem is the well-known autonomous nonlinear equation with nonhomogeneous initial conditions, giving free oscillations of a typical nucleus. This first-order system is a nonautonomous linear system with homogeneous initial conditions which governs the forced bubble growth. The second-order system consists of a linear autonomous differential equation and homogeneous initial conditions. It is needed to establish integrability conditions for the first-order solution.

The first-order solution is left for future research and the zeroth-order problem is analyzed in the phase plane. Then a novel approximate integration, $\tau = \tau(u)$, is given in terms of elliptic integrals and functions. We were not able to invert this solution and so the inverse $u = u(\tau)$ is found numerically. These data are then used to find an analytical approximation for use in future first-order calculations.

From: B. R. Parkin* and B. B. Baker**

Subject: Bubble Dynamics and Cavitation Inception Theory

Abstract: In order to provide some theoretical background and to motivate the more refined theory introduced below, we review some encouraging known theoretical results on bubble-ring cavitation inception. This review is followed by the development of the theory of bubble-ring cavitation cutoff. Its outcome, when compared with experiment, shows the need for a more refined inception theory.

The above comparison and the basic ideas behind the cutoff theory's formulation suggest a possible approach for a refinement based on a multiple scales expansion. This seems reasonable because the forcing function pulse in "laboratory time," t, varies slowly compared to the characteristic "bubble time," τ, which characterizes the response time of a typical microscopic cavitation nucleus. The ratio of these two times gives us a small parameter, ϵ, appearing in the forcing function, with the result that this problem involves only a soft excitation.

*Applied Research Laboratory and Aerospace Engineering, The Pennsylvania State University. **Now at the General Electric Company, Springfield, VA.

Expanding the forced Rayleigh-Plesset equation and its initial conditions to the second order in ϵ, we find that the zeroth-order problem is the well-known autonomous nonlinear equation with nonhomogeneous initial conditions, giving free oscillations of a typical nucleus. This first-order system is a nonautonomous linear system with homogeneous initial conditions which governs the forced bubble growth. The second-order system consists of a linear autonomous differential equation and homogeneous initial conditions. It is needed to establish integrability conditions for the first-order solution.

The first-order solution is left for future research and the zeroth-order problem is analyzed in the phase plane. Then a novel approximate integration, $\tau = \tau(u)$, is given in terms of elliptic integrals and functions. We were not able to invert this solution and so the inverse $u = u(\tau)$ is found numerically. These data are then used to find an analytical approximation for use in future first-order calculations.

Table of Contents

List of Figures

List of Tables

Nomenclature

C_p pressure coefficient = $(p - p_o)/(1/2)\rho V_o^2$.

C_{ps} pressure coefficient = $(p_s - p_o)/(1/2)\rho V_o^2$.

D hemispherical headform diameter.

γ air content parameter = $p_a/(2\sigma/R_o)$.

H maximum laminar separation bubble height.

K cavitation number = $(p_o - p_v)/(1/2)\rho V_o^2$.

p static pressure at any point in the flow.

p_a saturation dissolved air pressure.

p_o free-stream static pressure.

p_s static pressure in laminar separation bubble

p_v vapor pressure of water.

Q from bubble radius normalizer, (1 + Q), where Q = $(W_R)K/8$.

R(t) bubble radius at any instant.

Re diametral Reynolds number = V_oD/ν.

R_o free-stream nucleus radius.

r dimensionless radius = $R(t)/R_o$

ρ density of water.

s arc length along headform meridian.

σ coefficient of surface tension.

t "laboratory time."

τ "bubble time."

T_n slow-time scales = $\epsilon^n t$, n = 0, 1, 2, ...

u normalized bubble radius = r/(1 + Q)

V_{co} free-stream cutoff speed.

V_o free-stream velocity.

ν kinematic viscosity of water.

We diametral Weber number = $V_o/\sqrt{\sigma/(\rho D)}$.

W_R radial Weber number = $V_0/\sqrt{\sigma/(\rho R_0)}$.

Introduction

This paper reports some new beginnings in our efforts to apply the Rayleigh-Plesset[1*] theory of cavitation bubble dynamics to the prediction of cavitation inception on submerged bodies in flowing water at ordinary temperatures. For cavitation initiation under these conditions, we suppose that events leading to inception are sufficiently infrequent so that one can model the dynamics of cavitation-bubble growth as though each bubble were a small isolated isothermal spherical bubble containing a mixture of air and water vapor.

Thus in the interests of computational simplicity, we neglect the presence of neighboring walls and of adjacent bubbles. We also assume that cavitation is initiated from invisible air microbubbles of radius R_0 which are distributed throughout the flow. Past measurements[2] have shown that the population of such cavitation nuclei is highest for bubbles having a radius of only a few microns and that their numbers rapidly become smaller as their sizes increase. Of course, we know from potential theory that the minimum pressure in a flow occurs on the boundary and it is in just this region that inception is observed. Nevertheless we shall account for the presence of the submerged body upon the bubble dynamics chiefly by its pressure distribution and its boundary layer, retaining the simplification that the bubble motions show no other influence due to the wall. Even then we shall not be reticent about introducing further

*Superscribed numbers indicate citations in the References.

advantageous approximations for these and related flow or bubble properties.

Moreover, we shall consider only cavitating flows which fairly recently have received additional intensive experimental investigation[3,4,5]. Thus, we are relieved of the considerable effort required to calculate the noncavitating flow properties and we will also have a body of laboratory data which can be used to test the findings of the bubble dynamical calculations.

Past attempts to use "simple" bubble dynamics for the prediction of cavitation inception and the related scaling laws have generally met with disappointment. Therefore it is useful to confine our attention to our belief that the chief difficulty involves the proper use of bubble dynamics. By placing our trust in reliable experimental data about other things, we need not be distracted by the need to predict every single aspect of the flow from first principles; although we look forward to the day when this achievement will be realized with the help of computational fluid dynamics.

From the literature, one finds that the most extensive and consistent set of measurements has been made by a number of investigators on axially symmetrical headforms. Of these recent measurements, those data pertaining to cavitating and noncavitating flows around hemispherical headforms seem to be the most thoroughly reported. Consequently, we have chosen that flow configuration as the basis for the present analysis in spite of the fact that in the laboratory this flow generally exhibits a short laminar separation bubble downstream of the minimum pressure point as illustrated schematically in Fig. 1. This feature offers some advantages and some computational complexities in the present instance, and it suffers from the fact that the kind of cavitation inception which is associated with laminar separation is not found at Reynolds numbers usually encountered on ship propellers and other full-scale submerged bodies. Evidently we are dealing with a form of cavitation which is a laboratory artifact. Even so, the experimental data pertaining to the so-called *bubble-ring* cavitation are of a quality and consistency which permits them to be most useful to test the efficacy of various theoretical bubble-dynamical formulations.

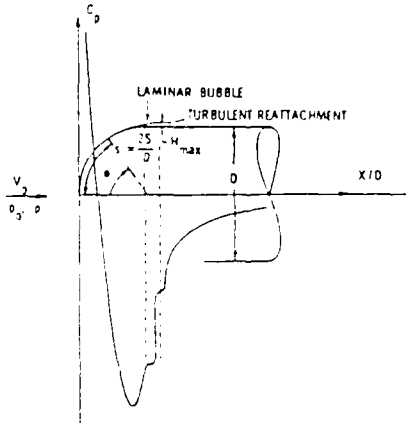

Figure 1.- Laminar separation on a hemispherical headform.

Theoretical Background

In a previous analysis of bubble ring cavitation[6], the senior author has suggested a sequence of key events that could lead to the inception of bubble-ring cavitation. The encouraging agreement between observed and calculated inception cavitation numbers suggests that those basic findings which result from a consideration of experimental observations, suggests that the following postulates could be true, at least in their major respects.

(a) Thus, it is supposed that a typical free-stream nucleus enters the boundary layer at some point ahead of the minimum pressure on the body and moves with a convective speed characteristic of that flow region.

(b) After arriving at the point on the body where the absolute value of the pressure coefficient equals the cavitation number, the nucleus undergoes vaporous growth, reaching a maximum radius down stream of the minimum pressure point.

(c) The vapor bubble then becomes fixed at a point inside the laminar separation bubble ahead of the turbulent reattachment region. It can then experience further growth by air diffusion from the water into the cavitation bubble because the static pressure in the

laminar separation bubble is generally greater than the vapor pressure and further vaporous growth will not occur.

(d) This gaseous growth ends when the cavitation bubble radius becomes large enough to interact with the free-shear layer at the edge of the laminar bubble.

(e) This interaction causes the cavitation bubble to be removed from the separation region and to move with the local flow into the turbulent reattachment region at the end of the laminar bubble. Turbulent eddies in the reattachment region produce additional low pressures in the water which can promote further vaporous growth.

(f) In any case, the intense shearing action within this turbulent flow may distort and tear the cavitation bubbles and this leads to a small white band or cloud of small bubbles which is easily seen and heard.

This visible state of inception or desinence is called *bubble-ring* cavitation. It is not to be confused with a more developed cavitation state, in which the laminar separation region is filled with little attached glassy cavities. This latter form is actually a miniature free-streamline or cavity flow and it is called *band* cavitation.

Once the gaseous growth in the laminar separation zone is established, the conditions for the onset of bubble-ring cavitation are present and all events experienced by a typical nucleus in its later stages of development occur automatically. The separation zone does insure a favorable environment for gaseous growth because the water is definitely supersaturated in this region. It is also found that the most favorable condition for gaseous growth occurs when the vapor bubble just attains its maximum radius and simultaneously arrives at the laminar separation zone. The accelerations in the liquid surrounding the cavitation bubble increase the degree of supersaturation at the bubble wall over that which would exist if the accelerations were negligible. Therefore the probability that the cavitation bubble can become stabilized at a fixed point in the laminar separation zone would be greatest at this instant.

Consequently, the process of initial vaporous growth is the only process of bubble-ring cavitation needing detailed analysis. A legitimate question to be asked at this point is why not let a computer do the analysis for us by means of a standard numerical method such as a Runge-Kutta routine? After all, this problem involves only an ordinary pulsed Rayleigh-Plesset differential equation.

There are two important reasons for embarking upon a program of analysis. First, cavitation inception is characterized by critical values of the flow parameters such as the free-stream velocity, V_0, the headform diameter, D, the cavitation number, $K = (p_0 - p_v)/(1/2)\rho V_0^2$, the free stream static pressure, p_0, the liquid vapor pressure, p_v, density, ρ, viscosity, μ, and surface tension, σ, as well as the dissolved air content and also perhaps by a typical nucleus radius, R_0, or a probability distribution of nuclei sizes.

It is our aim to find critical values of these parameters, singly or combined as in the cavitation number, Reynolds number and/or Weber number, etc., which define cavitation onset. And of course, the form of the forcing function in any particular instance will also play a role in all of this. When one considers the large number of these parameters, it is apparent that successive numerical integrations for the many cases of interest is not likely to be fruitful from the viewpoint of basic understanding of any inception process even if the work were to be done.

Second, the nonlinearity of the Rayleigh-Plesset differential operator makes the task of relating critical flow parameters to the calculated growth curves, R(t), very demanding because of the extreme accuracy required[6]. For example, it has been known for some time that this differential equation can have solutions of different classes or forms, depending upon the values chosen for the basic pulse forcing-function parameters. Figure 2 illustrates the kind of things that can occur. This figure, in two parts, shows transient responses of an isothermal nucleus to parabolic pulses of various pulse heights, β, as indicated,

but having a fixed duration $\theta = 0.4$.* It is seen that illustrations (a) and (b) in Fig. 2 have different scales on both axes and that the curves in (b) start at values of time, τ, where the curves of (a) stop. The different scales of the two drawings prevent us from joining them into a single illustration. The reason for this scale difference can be appreciated from the fact that the ordinate of each drawing is the natural logarithm of the dimensionless radius, $r = R(\tau)/R_0$. As we look at some of these curves, it is clear that $r(\tau)$ varies by as much as a thousand fold.

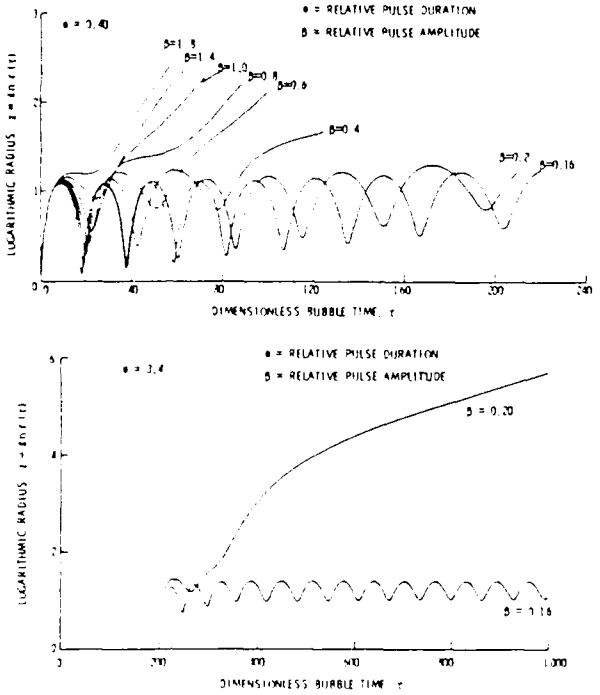

Figure 2 - Isothermal cavitation bubble growth curves in response to single parabolic-pulse forcing functions

(a) Shorter growth periods.

(b) Longer growth periods

*This notation should not be confused with later usage in which some of these symbols will have different meanings. These unpublished results were obtained in about 1954 by the senior author from a series of Reeves analogue computer runs at JPL. They were obtained under the direction of M.S. Plesset. The work was sponsored by the late Phillip Eisenburg, then head of the Mechanics Branch, ONR.

On the other hand, some curves show essentially no net growth. The bubbles in this case experience a nonlinear oscillation having a total displacement of about four as can be seen in (b) for $\beta = 0.16$. If the value of β is changed from 0.16 to 0.20, the vapor bubble shows explosive growth. Near $\tau = 1000$ the growth curve seems to approach an asymptotic growth rate having a nearly linear $r(\tau)$. Evidently, these contrasting solutions give us a glimpse of the kinds of responses that can occur and we are left to wonder about the precise value of β, between 0.16 and 0.20, which marks the transition between these two radically different solutions.

This situation would not be particularly bad if it were not for the fact, already noted, that in some cases very small changes in the various parameter values can have extraordinarily large and unexpected effects on the nature of the bubble growth[6]. Since the estimation of these critical parameters requires a certain amount of *a priori* knowledge, we conclude that even a crude analysis, if it can be properly executed, can be better than none at all. At this time, all we can offer regarding the appropriateness of one or another analytical approach is how well it compares with experiment.

Recently, one such analysis for bubble-ring cavitation[6] has shown rather good agreement between analytical estimates and observed trends of cavitation inception (or desinence, in the experiments). These results are shown in Fig. 3 where the incipient cavitation number is plotted for a range of free-stream velocities. The figure shows the calculated values to be sensitive to the ratio of maximum vapor bubble diameter, $2R_{|max}$, and to laminar separation bubble height, H. Better agreement between calculated and experimental findings could be shown had we permitted the ratio, $\theta = 2R_{|max}/H$, to exceed unity But since the theory has been greatly simplified, it seems that agreement between experimental and theoretical trends is the main point to be exhibited. The basic information on laminar bubble heights used here is a synthesis of available experimental data as shown in Fig 4.

The basic scaling equation seen in Fig. 3 was found to be

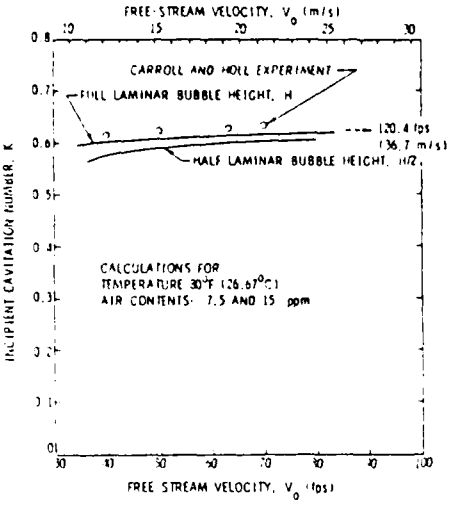

Figure 3.- Cavitation inception on a hemispherical headform.

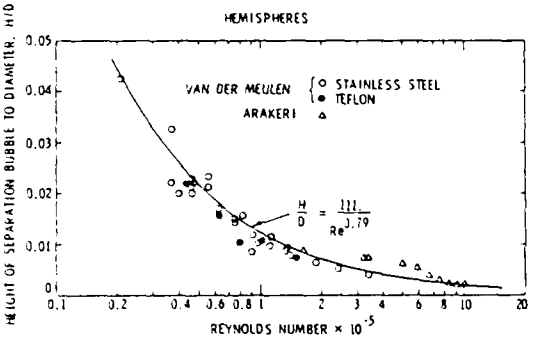

Figure 4.- Laminar separation bubble heights on a hemispherical headform.

$$K = -C_{p_s} - (Re^{0.79}/13.875\theta We^2) \times [\,1 - \gamma(R_0/55.5\theta D)^2\, Re^{1.58}\,], \qquad (1)$$

where the Reynolds number, $Re=V_0D/\nu$, is based on headform diameter, D, and the kinematic viscosity is $\nu=\mu/\rho$. The Weber number, $We = V_0/\sqrt{\sigma/(\rho D)}$ is also based on headform diameter. The dissolved air content parameter, $\gamma = p_a/(2\sigma/R_0)$, is seen to be the ratio of the free-stream saturation value of the partial pressure of dissolved air, p_a, to the free-stream nucleus surface-tension pressure, $2\sigma/R_0$. In most laboratories this partial pressure in the free stream is measured by a Van Slyke apparatus. The quantity C_{p_s} is the pressure coefficient on the headform at the point of laminar separation.

An interesting further aspect of bubble-ring cavitation following from Eq. (1) is that the dissolved air content has practically no influence on the inception cavitation number when the temperature is held constant. This same conclusion had already been reached by Carroll and Holl[4] as a result of their experiments. The reason for this situation indicated by Eq. (1) can be seen from the fact that in the square brackets the quantity R_0^2 is present. This quantity is very small compared to unity and so it is found that the entire term, $\gamma(R_0/55.5\theta D)^2Re^{1.58}$, is much less than unity over the Reynolds number range of interest here. Consequently, one makes very little error by writing

$$K = -C_{p_s} - (Re^{0.79}/13.875\theta We^2) \qquad (1a)$$

in place of Eq. (1).

We can not conclude however, that the theory would still be useful if we were to put $\gamma=0$. If the water contains no dissolved air, postulates (d) through (f) would have no physical basis. Then there can be no gaseous bubble growth and it is doubtful that bubble-ring cavitation would exist. Thus, there must be some air in the water if bubble-ring cavitation is to be expected.

We have observed that a typical free-stream nucleus, which participates in the events leading to bubble-ring cavitation, has a very small size. That this might be the case was inferred by matching the findings of the theory with a phenomenon peculiar to bubble-ring cavitation which we will call *cavitation cutoff*.

Cavitation cutoff was observed first by Carroll and Holl in their experiments and found independently by Kodama* at about the same time. It was found by all of them that there is a lower limiting free-stream "cutoff" velocity for bubble-ring cavitation on hemispherical headforms. At lesser speeds bubble-ring cavitation disappears altogether, although other forms such as band cavitation may be present. Our cutoff-speed matching calculations indicated that the radius of the *typical participating nucleus* in the Holl-Carroll experiments was about 5 - 7 microns. Aside

*Private communication, 1979.

from a report to the sponsor, this theoretical development has not been given wide dissemination. Therefore, it seems appropriate to present it here.

Cavitation Cutoff

Basic Ideas

As a first step in calculations for cutoff, we offer an interpretation of the experimental findings which can be expressed in terms of the present theory. One possibility may be that because the cutoff speed is a relatively low speed, the cavitation number at this speed should be less than that seen at higher speeds. The idea here is that since the dynamic pressure is less at a lower speed, the free stream static pressure must also be reduced in order to promote vaporous bubble growth. Now, the bubble-ring cutoff speed means that if the free stream velocity is lowered still farther no matter what is done with the free stream static pressure, bubble-ring cavitation is not observed, although other forms may still appear. But as the free-stream static pressure is lowered the maximum vapor bubble size initially stabilized in the laminar separation region will increase. Therefore we suggest that the vaporous cavitation bubble is limited to a greatest maximum size. According to postulate (d) of the "theoretical background" section this size must depend on the laminar free-shear layer height, H. That is, there will be little or no gaseous growth phase at bubble-ring cutoff speed. Instead the vapor bubble is swept almost immediately into the tubulent reattachment zone. This line of reasoning suggests that the limiting condition leading to bubble-ring cavitation cutoff can bewritten as

$$2R_{|max} \approx H \qquad (2)$$

Figure 4 above illustrates that a satisfactory representation of the van der Meulen and Arakeri data on laminar bubble height is given by

$$H/D = 111/Re^{0.79}. \qquad (3)$$

Since the maximum cavitation bubble diameter is to equal θH and if we introduce the dimensionless cavitation bubble radius,

$$r_m = R_{|max}/R_0,$$

we can write

$$r_m = 55.5\theta D/R_0 Re^{0.79}. \qquad (4)$$

The parameter θ is at our disposal. Again, the idea here is that the greatest amount of vaporous growth consistent with the key postulates of bubble-ring cavitation theory is limited by the height of the laminar bubble.

Aproximate Forcing Function

Recall next that the crucial simplification introduced into the crude theory under review is that the actual forcing function for vaporous growth is replaced by one positive step function starting with a positive jump of

$$\alpha = -(C_{p_{min}} + K)/C_\sigma, \qquad (5)$$

where C_{pmin} is the minimum pressure coefficient on the headform and C_σ is the dimensionless coefficient,

$$C_\sigma = 4\sigma/R_0\rho V_0^2. \qquad (6)$$

After a short dimensionless elapsed "bubble time", τ_0, measured in units given by

$$\tau = [t\sqrt{2\sigma/\rho R_0^3}], \qquad (7)$$

the first jump is followed by a negative jump of magnitude

$$\beta = (K + C_{ps})/C_\sigma, \qquad (8)$$

at $\tau = (\tau_a + \tau_0)$. This "piecewise autonomous" approximation is illustrated in Fig 5. Adopting this approximation, we can write the dimensionless forcing function, $F_a(\tau)$, as,

$$F_a(\tau) = \begin{cases} 0, & 0 \le \tau \le \tau_a, \\ \alpha, & \tau_a \le \tau \le \tau_a + \tau_0, \\ \beta, & \tau_a + \tau_0 \le \tau \le \tau_m. \end{cases} \qquad (9)$$

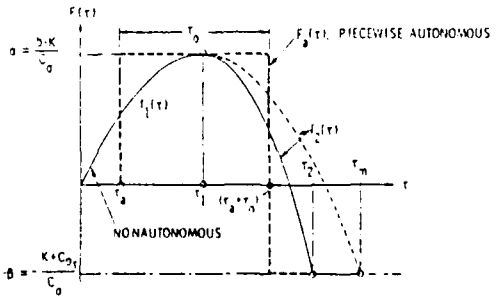

Figure 5.- Forcing functions for the "piecewise-autonomous" approximation.

Formulation of the Theory

Next we write the Rayleigh-Plesset equation as the first-order pair,

$$v = dr/d\tau ,$$

$$(2r^2)^{-1}d(r^3v^2)/dr = \gamma/r^3 - 1/r + F_a(\tau) , \quad (10)$$

with

$$v(0) = dr(0)/d\tau = 0 \text{ and } r(0) = 1 .$$

The air content parameter γ has been defined in the discussion of Eq. (1). Multiplying both sides of Eq. (10) by $2r^2$ and integrating formally from $r = 1$ to $r = r_m$, we find that

$$r_m^3 v_m^2 = 2I_a(r_m) + 2\gamma \ln r_m - (r_m^2 - 1), \quad (11)$$

where

$$I_a(r_m) = \int_1^{r_a} r^2F_a(\tau)dr + \int_{r_a}^{r_o} r^2F_a(\tau)dr + \int_{r_o}^{r_m} r^2F_a(\tau)dr$$

$$= (1/3)[(\alpha + \beta)(r_o^3 - 1) - \beta(r_m^3 - 1)].$$

Applying all of this to Eq. (10) , we get

$$r_m^3 v_m^2 = (2/3)(\alpha + \beta)r_o^3 - (2/3)\alpha - (2/3)\beta r_m^3 + 2\gamma \ln r_m - (r_m^2 - 1) . \quad (12)$$

Next one observes that solutions for which the bubble just achieves its maximum radius, r_m, after $F_a(\tau)$ first equals $-\beta$ requires that phase-plane trajectories indicating unlimited vaporous growth are not admissible solutions. Moreover one can argue that the demarcation between these unwanted trajectories and those leading to bounded (periodic) solutions is the separatrix through the saddle point on the phase-plane r axis at $(r_c,0)$. We shall call the saddle point location the critical point, and we shall denote the values of β and α at this point by α_c and β_c .

It is known that the bubble time, τ, required for the radius, $r(\tau)$, to reach the saddle point along the separatrix is infinite. But it turns out that $F(\tau)$ is such that the time available in units of "fast" time from $\tau=0$ to $\tau=\tau_m$ is very long, even though the corresponding period in laboratory or "slow" time is very short because of the conversion factor between the two shown in Eq. (7) . This means that the actual time available, as defined by $F(\tau)$, will place all actual trajectories very close to the separatrix. Moreover the values of α and β borne by these trajectories will in fact, be almost indistiguishable from α_c and β_c . Consequently, we make negligible error in most situations of interest if we replace the actual α and β by α_c and β_c . This implies that we give up the possibility of matching the time available for a prescribed growth, r_m, with the time actually needed to obtain it. This simplification contains an extremely small error and it offers a straightforward way for us to find $r_c = r_m$, α_c and β_c .

In the phase plane the saddle point is found from the conditions that $v_c=0$ and $[dv/dr_m]_{(r=r_m)} = 0$. From an application of these to Eq. (12), we find

$$0 = (2/3)(\alpha_c + \beta_c)r_o^3 - (2/3)\alpha_c - (2/3)\beta_c r_m^3 + 2\gamma \ln r_m - (r_m^2 - 1) \quad (13)$$

and

$$\beta_c = [(\gamma/r_m^2) - 1]/r_m . \quad (14)$$

Equations (13) and (14) start us toward the determination of the cavitation cutoff speed. They do, however, contain the unknowns r_o and α_c, because if for now we regard $V_0 = V_{co}$ as known, and rewrite Eq. (4) as

$$r_m = 55.5\theta D^{0.21}\nu^{0.79}/(R_o V_{co}^{0.79}) , \quad (4a)$$

then Eq. (4a) determines r_m provided R_o is also regarded as being known. But β_c is determined by Eq. (14). Adding Eqs. (5) and (8), and regarding α and β as critical values, one finds that

$$\alpha_c + \beta_c = (C_{p_{min}} + C_{p_s})/C_\sigma . \quad (15)$$

Again we consider the factors, R_o and V_o, appearing in C_σ as the known nucleus radius and cutoff speed. Then, α_c is also determined and r_o can be found from Eq. (13) because all other parameters in Eqs. (13), (14), (4a) and (15) are known. These equations define a functional relationship between V_{co} and R_o .

It may seem that the foregoing analysis completes our study of bubble-ring cavitation cutoff speed. This is not quite true however, because we have imposed no condition which insures that the value of V_{co} corresponds to the lowest possible cavitation number. The following arguments are needed to do this and thereby to satisfy all physical conditions indicated at the outset.

We start with the observations that situations can arise in which the duration of the pulse, τ_0, is so long in terms of bubble time that the phase-plane saddle point, r_c, is even less than r_0. This is almost as though we had let τ_0 and therefore $r_0 \to \infty$, thereby reducing the problem to the familiar autonomous single step-function problem . In such a case the limiting values of r_m will be associated with a new critical value of α_c which will be less than the critical value of α_c borne by the separatrix found above and which we found to depend on β_c. Arguments only slightly different from those given previously can be used to show that

$$\alpha_c = [(\gamma/r_c^2) - 1]/r_c,$$

with the analogue of (13) being

$$0 = (2/3)\alpha_c(r_c^3 - 1) + 2\gamma \ln r_c - (r_c^2 - 1).$$

Eliminating α_c between this pair of equations we get a single equation for the determination of r_c:

$$r_c + 2\gamma(1 - 3 \ln r_c) - 3 - 2[(\gamma/r_c^2) - 1]/r_c = 0. \quad (16)$$

Because $\alpha_c > |\beta_c|$, the present value of r_c will be less than the previous value. Therefore we call it the smaller of the two critical radii. The closed trajectories to the left of r_c will certainly lead to motions having short periods and very small amplitudes. In order to insure that larger amounts of vaporous growth are produced, the phase-plane trajectories starting from the initial point will follow paths which are outside the new separatrix and they will bear larger values of α than the α_c just found. And since $-C_{p|_{min}}$ is fixed, the K values borne by these trajectories will be less than that found on the α_c trajectory. Moreover, if we put $r_0 = r_c$ we will have reduced τ_0 to its shortest possibile duration and this requires the lowest possible K value to achieve the desired vaporous growth. Therefore we can modify (16) to read

$$r_0 + 2\gamma(1 - 3 \ln r_0) - 2[(\gamma/r_0^2) - 1]/r_0 = 3, \quad (17)$$

again, because it is found that the true values of α are practically indistinguishable from α_c. For values of r_0 in the interval $(1, r_m)$, Eq. (17) will have one root provided that V_{co} is properly chosen. The fact that r_0 depends parametrically on V_{co} suggests that we should rewrite (17) as

$$G(V_{co}) = r_0 + 2\gamma(1 - 3 \ln r_0) - 2[(\gamma/r_0^2) - 1]/r_0 - 3 = 0, \quad (17a)$$

and solve for G = 0 by iteration on V_{co} because Eqs. (13), (14), (4a), (15), and (17) now form a closed system.

Cutoff Calculations

As indicated previously, this solution will depend upon the value of R_0 which is taken as being known. Then one can use this value and the corresponding value of V_{co} to find C_σ from Eq. (6). Once this has been done one can find the cavitation number, Reynolds number and all other parameters pertaining to this particular flow condition. A fairly extensive series of calculations has been carried out in order to test the preceding theory against the cutoff experiments of Carroll and Holl on a 2-inch (0.0508 m) diameter headform. The detail available to us regarding Kodama's experiments was insufficient for us to use his results to test the theory further although his findings seem to be consistent with the observations of Holl and Carroll[5]. At an air content of 7.8 ppm and 80°F (26.67°C), Holl and Carroll observed bubble-ring cavitation at 40 ft/sec (12.192 m/sec) but no bubble-ring cavitation at the next lower test speed of 30 ft/sec (9.144 m/sec), indicating a cutoff speed somewhere between these two values.

Calculated cutoff data for V_{co} on a 2-inch (0.0508 m) diameter headform at a temperature of 80°F (26.67°C) and $C_{p_s} = -0.630$ are tabulated below to show the corresponding radius R_0 of a "typical" participating nucleus at two air contents. and values of V_{co} expressed in feet per second.

Table I - Participating Nucleus Size

V_{co} ↓	Air Content, ppm.	
	7.5	15.0
30	5.65	4.28
40	4.71	3.61
	R_0	

V_{co} = 9.144 & 12.192 m/s

In contrast to the findings of Eq. (1), Table I shows at cavitation cutoff that the nucleus size is sensitive to the dissolved air content. For a given cutoff speed, the value of R_0 decreases with increasing air content. At fixed air content, the value of R_0 decreases with increasing cutoff speed. Comparison of these tabulated results with the Holl-Carroll data suggest that an appropriate diameter of the typical participating nucleus which will fit the calculated results to the experiments should be between 9 and 11 microns. This is at the small end of experimentally determined distribution data in water tunnels and suggests that there can be many nuclei within the size range which may permit the occurrence of bubble-ring cavitation. The calculations from Eq. (1) leading to the results shown in Fig. 3 were carried out for an R_0 of 5.18 microns.

Holl and Carroll also discovered a temperature dependence of bubble-ring cutoff cavitation number with Reynolds number. Calculations which included the influence of temperature on R_0, seemed to exhibit the same qualitative trends as the observations but the calculated results did not display the same degree of temperature sensitivity, Fig.6. In these calculations the physical parameters which were taken to vary with temperature were the Henry's law constant, the surface tension, the vapor pressure and the kinematic viscosity of the water. Evidently, other factors should be considered to complete the theory.

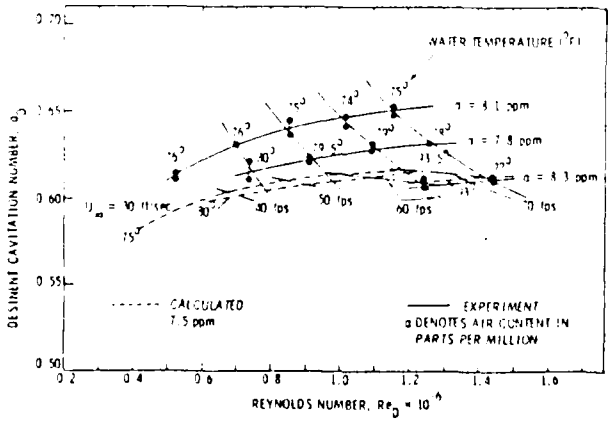

Figure 6 - Observed and calculated temperature effect on cavitation cutoff.

Because of its several successful predictions so far, the bubble dynamical approach to understanding this one type of inception, argues for its further refinement in order to remedy the above and other shortcomings in the method. The most obvious topic for further study is the development of a more realistic treatment of the bubble dynamics which might be capable of lessening the observed deficiencies. The following discussion, outlining some research in progress, summarizes our first attempt to address this aspect of the problem.

The Refinement

The Flaccid Bubble and Initial Conditions

A minor refinement to the bubble dynamical theory underlying the preceding cutoff calculations is that we can investigate possible benefits that a more accurate representation for the initial conditions of vaporous growth might provide. Generally this refinement is honored by its neglect. Then one simply starts with the undisturbed free-stream nucleus and puts $R(0) = R_0$ and $(dR/dt)_{t=0} = 0$, because in many cases of interest the solutions for unlimited growth, as illustrated in Fig. 2b, are sought. The precision of the initial conditions is then of little consequence. This situation does not apply here because, now the vaporous growth is limited by the separation bubble height.

On the other hand the flow over a body produces static pressures on the surface which differ from the free-stream value. In particular, the static pressure at the point on the body at the start of vaporous growth is given by $C_p = -K$, corresponding to a free-stream static pressure of p_0. For an isothermal flaccid bubble, we have $p_g R(0)^3 = p_a R_0^3$ from Boyle's law. This relationship represents a shorthand way of saying that a free-stream nucleus enters the boundary layer and is conveyed, as an air bubble without any vaporous growth, to the point where $C_p = -K$, and then vaporous growth starts.

Next we can calculate the force balance across the bubble surface when it is in the free-stream and the outside static pressure is

p_0. Then $p_0 = p_v + p_a - 2\sigma/R_0$. If $p(0)$ is the pressure outside the bubble at the location where vaporous growth starts, the force balance is $p(0) = p_v + p_g - 2\sigma/R(\tau)$. The gas pressures in these equations can be found directly and these pressures substituted into Boyle's law above. In doing this we employ the various dimensionless quantities used in Eqs. (1) and (1a) and we introduce the new parameter, W_R, the Weber number based on R_0 and write $W_R = V_0/\sqrt{\sigma/(\rho R_0)}$. After further manipulation of Boyle's law we get

$$[(C_p + K)W_R/4]r^3 + r^2 - 1 - (W_R)K/4 = 0. \quad (18)$$

Eq. (18) is the flaccid bubble equation which holds on the surface of the body. When $C_p = -K$ and $r = r(0)$, we can solve the resulting quadratic to get

$$r(0) = \sqrt{1 + [(W_R)K/4]} \approx 1 + (W_R)K/8 = 1 + Q. \quad (18a)$$

Eq. (18a) gives the initial value of r and we write $Q \equiv (W_R)K/8$.

Our next task is the development of an expression for $dr/d\tau$ and its evaluation at that point on the body where $C_p = -K$. The known quantity on the headform is $C_p(s)$, from which the local flow velocity just outside the boundary layer can be found. Then, in keeping with the simplification that the boundary layer is a vortex sheet we put the convective speed, V(s), equal to one half of the outer flow speed. In addition, if ds is an increment of dimensionless arc length and dS is the same increment measured in suitable length units we can write $ds = dS/(D/2)$. Thus

$$V(s) = dS/dt = (D\,ds/2)/dt$$

and

$$ds/dt = (V_0/D)\sqrt{[1 - C_p(s)]}. \quad (19)$$

Now we can write

$$dr/d\tau = (dr/dC_p)(dC_p/ds)(ds/dt)(dt/d\tau).$$

The first factor in this product can be found by implicit differentiation of Eq. (18), the second from the equation for $C_p(s)$, the third from Eq. (19), and the fourth from Eq. (7). After a certain amount of manipulation and the use of $C_p = -K$ in the appropriate places, we find an expression for $(dr/d\tau)_{(\tau = 0)}$. This expression contains certain terms requiring r(0) from Eq. (18a) in order to complete the calculation of the initial bubble growth rate. When appropriate values of all physical and geometric quantities are used in the growth-rate equation, $(dr/d\tau)_{(\tau = 0)}$ is found to be extremely small compared to other quantities in the theory. Therefore we make practically no error if we take the second initial condition to be null:

$$(dr/d\tau)_{(\tau = 0)} = 0. \quad (20)$$

Nevertheless as we shall see later, it is of conceptual value to understand that actually this initial growth rate is a very, very small positive number.

Forcing Functions

As we have already indicated from the beginning, vaporous bubble growth starts when $C_p(s) = -K$ and the dimensionless bubble time or fast time, τ, is zero. Let the dimensionless arc length on the body be s_0 at that point. Its value can be found from the value of K. But this value varies and we need to allow for that in defining the forcing function because both its amplitude and duration are influenced by that value. On the other hand we can select a likely range for K depending on the flow conditions or from the data of Holl and Carroll. Therefore we can use their experimental pressure distributions in order to define an average pressure distribution for the free-stream velocity range of interest. We can pick some point, s_1 say, at which $C_p(s_1) > -K$ and we can then adapt Eq. (19) in order to define a relationship between s and a quantity τ^* that is invariant with respect to K. Clearly, the required relationship is

$$\tau^*(s) = (D/V_0)\sqrt{(2\sigma/\rho R_0^3)} \int_{s_1}^{s} dx/\sqrt{[1 - C_p(x)]}. \quad (21)$$

Equation (21) is used to carry out numerical integrations based directly on individual points from the Carroll-Holl data. Therefore one selects s_1 to be the first datum point in or near the range of interest, $C_p(s_1) \approx -K_{max}$, and integrates numerically point by point over the rest of the points, $s_i > s_1$, in the data set. The result will be a table of s_i and $C_p(s_i)$

versus τ^*_i, where the index i starts at 1 and ranges over all points indicated above. Then one can plot the points $C_p(\tau^*_i)$ in $(\tau^*_i, -C_p)$ coordinates. Next he can define displaced (τ, F) coordinates in which the origin is positioned at that value of τ^* for which $C_p(\tau^*_i) = -K$ and in which $F = -(C_p + K)$. If the minimum value of C_p is $C_{p\,|min}$ then the greatest value of F is $F_{max} = (-C_{p\,|min} - K)$. The displacement of the (τ, F) system with respect to the $(\tau^*_i, -C_p)$ coordinates can be found by means of parabolic interpolation in the $(\tau^*_i, -C_p)$ plane. Indeed, if the interpolation formula covers an adequate range of cavitation numbers, the formula can be written down once and for all and arranged to give the displacements $K - C_p(\tau^*_i)$ and $\tau^*(K) - \tau^*_i$ for each value of K used in any particular computation. Thus we will get a new forcing function every time K changes its value.

In any case a table of points, τ_i versus F_i, results from these calculations as shown in Fig. 7. Our aim has been to preserve the Holl-Carroll data points themselves as far into the calculation as possible and we shall write any member of the family of forcing functions symbolically as $F(\tau_i ; K)$. The faired curve through the points in Fig. 7 results from a sequence of parabolic interpolations between experimental points. The next step is to fit the points defining $F(\tau_i ; K)$ with a suitable continuous function designated by $F(\tau ; K)$. This step will be deferred to a later point in the argument, however. Having arrived at the initial conditions and the forcing function for vaporous growth, we turn next to the differential equation governing the process and to the statement of the mathematical problem to be addressed.

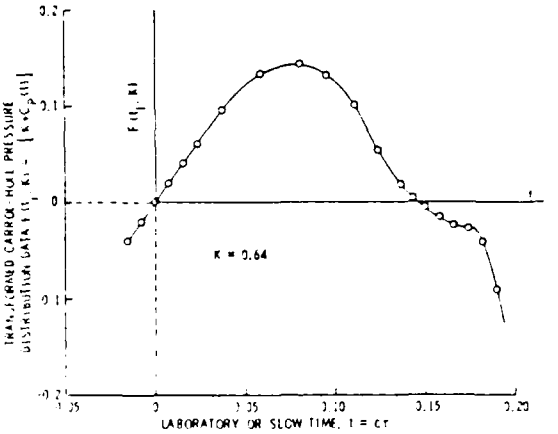

Figure 7.- Holl-Carroll forcing-function data.

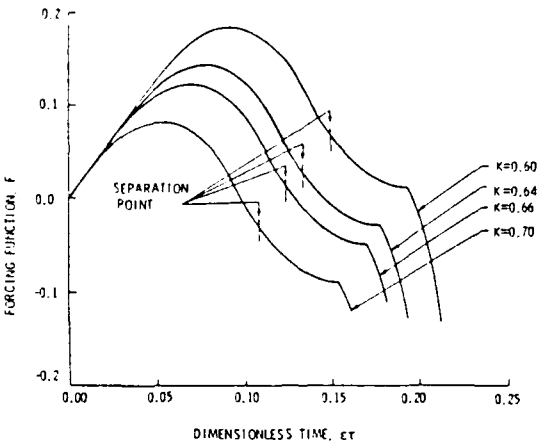

Figure 8.- Forcing-function family members for various cavitation numbers.

The Initial-Value Problem

All ingredients for the statement of the initial value-problem are given by Eqs. (10), (18a), (20) and the continuous form of the forcing function, $F(\tau ; K)$ as just described. Rewriting Eq. (10) as a single second order equation and assembling the remaining results we may state the initial-value problem as

$$r(d^2r/d\tau) + (3/2)dr/d\tau = \gamma/r^3 - 1/r + [(1/2)\rho V_0^2/(2\sigma/R_0)]F(\tau; K)$$

$$r(0) = \sqrt{[1 + \{[(W_R)K/4]\}} \approx 1 + (W_R)K/8 = 1 + Q. \quad (22)$$

$$(dr/d\tau)_{|(\tau = 0)} = 0.$$

Recall that the air content parameter is defined in remarks immediately following Eq.(1). Aside from the initial condition and the family of forcing functions, Fig. 8, which are specific to this discussion, Eqs. (22) exhibit the customary dimensionless form of the initial value problem for the Rayleigh-Plesset equation.

It is convenient to normalize the initial condition on the radius in Eqs. (22) so that it reads $u(0) = 1$. If we put $r = (1 + Q)u$, this

substitution will certainly normalize the r(0) initial condition and the initial value problem will now read

$$u(d^2u/d\tau^2) + (3/2)(du/d\tau)^2 = \gamma/[(1+Q)^5u^3] - 1/(1+Q)^3u + f(\tau; K)/(1+Q)^2, \quad u(0) = 1, \quad (du/d\tau)_{(\tau=0)} = 0, \tag{22a}$$

where

$$f(\tau\,;\,K) \equiv [(1/2)\rho V_0^2/(2\sigma/R_0)]F(\tau; K).$$

These normalized equations are the basis of the subsequent analysis.

Multiple Scales Representation

The possibility that a multiple scales analysis might be useful for the present problem follows from the fact that a fast time, τ, as defined by Eq. (7), giving the transformation between bubble time and laboratory or slow time, t, can be seen. Moreover, the foregoing analysis shows clearly that the scale of the slow time is defined by the convective process which converts the pressure distribution on the body into the bubble-dynamical forcing functions as indicated by Eqs. (19) and (21). If we write T to represent the laboratory time scale, in which t is measured, it is clear from Eq. (21) that $T = D/V_0$. Similarly, we can denote the time scale of bubble time by $[\tau]$ and write $[\tau] = R_0\sqrt{\rho R_0/2\sigma}$ which, aside from a numerical factor O(1), measures the period of free oscillations of a cavitation nucleus. A small parameter ϵ can be formed from the ratio, $[\tau]/T$. Thus,

$$\epsilon = [(V_0R_0)/D]\sqrt{\rho R_0/2\sigma}. \tag{23}$$

A very rough estimate indicates that ϵ will be about 1/1000. Evidently the conversion of dimensionless bubble time, τ, to laboratory time, t, is $\epsilon\tau = t$. Here the laboratory time is taken to be dimensionless as represented by the integral in Eq. (21) or by the ratio τ/T, for example. To recapitulate, we observe that the two time scales characterizing cavitation inception in the flow on submerged bodies are $t = \epsilon\tau$ and τ.

The next step in the analysis is to represent the dependent variable, $u(\tau,\epsilon)$, as is customary, by an expansion in powers of ϵ and with independent variables

$$T_n = \epsilon^n\tau, \quad n=0, 1, 2, \ldots .$$

Therefore we write

$$u(\tau,\epsilon) = u_0(T_0, T_1, T_2, \ldots) + \epsilon u_1(T_0, T_1, T_2, \ldots) + \epsilon^2u_2(T_0, T_1, T_2, \ldots) + \ldots . \tag{24}$$

Since we shall carry out the expansion to order ϵ^2, we require only the independent variables, T_0, T_1 and T_2 in subsequent work. The chain rule is used to express the derivatives, $du/d\tau$ and $d^2u/d\tau^2$, appearing in Eqs. (22a) in order to insure that the resulting multiple scales expansion is consistent in its powers of ϵ. For example, the initial condition, $u(0) = 1$, takes the form $u_0(0) - 1 + \epsilon u_1(0) + \epsilon^2u_2(0) = 0$ for all ϵ. Therefore, $u_0(0) = 1$ is the only nonzero initial condition among the u_n. Slightly more involved reasoning shows that all initial conditions among the $du_n/d\tau$ are null.

Turning now to the forcing function as defined in connection with Eqs. (22a), we see that $f(\tau\,;\,K)$ actually depends on the laboratory time, $t = \epsilon\tau = T_1$, only. Consequently, one expects that it should be represented as a *first-order* quantity, $f(\tau\,;\,K) = \epsilon g(\tau\,;\,K)$, where the function g is designed to provide a suitable analytic approximation to the Holl-Carroll experimental pressure distribution as illustrated in Fig. 8. A likely choice for the form of this "soft" forcing function is deferred until later.

It remains to apply the method of expansion discussed above and to present the system of equations, representing the initial value problems of zeroth, first and second orders in ϵ. The derivation of these results is tedious and we will write them down without further ado.

$O(\epsilon^0)$:

$$u_0(d^2u_0/d\tau^2) + (3/2)(du_0/d\tau)^2 = \gamma/[(1+Q)^5u_0^3] - 1/(1+Q)^3u_0, \quad u_0(0) = 1, \quad (du_0/d\tau)_{(\tau=0)} = 0. \tag{25}$$

$O(\epsilon^1)$:

$$d^2u_1/d\tau^2 + [(3/u_0)\,du_0/d\tau]\,du_1/d\tau + [(4/u_0)\,d^2u_0/d\tau^2 + [9/(2u_0^2)](du_0/d\tau)^2 + 2/[(1+Q)u_0)^3]\,u_1 = [\tau/(u_0(1+Q)^2)]\,g(\tau\,;\,K), \tag{26}$$

$u_1(0) = 0,$

$(du_1/d\tau)_{(\tau=0)} = 0.$

$O(\epsilon^2)$:

$$d^2u_2/d\tau^2 + [(3/u_0)\,du_0/d\tau]\,du_2/d\tau + \{[(4/u_0)\times d^2u_0/d\tau^2 + [9/(2u_0^2)]\,(du_0/d\tau)^2 + 2/[(1+Q)u_0]^3\}u_2 = 3\{\tau u_1/[(1+Q)u_0]^2\}\,g(\tau\,;K) - H(\tau).$$

$u_2(0) = 0,$

$(du_2/d\tau)_{(\tau=0)} = 0,$ (27)

where

$$H(\tau) = u_1^2/[(1+Q)^3u_0^4] + [4u_1/u_0]\,d^2u_1/d\tau^2 + 6u_1/[(1+Q)u_0^2]\,d^2u_0/d\tau^2 + [3/2u_0](du_1/d\tau)^2 + 9[u_1/u_0^2](du_0/d\tau)(du_1/d\tau) + [9u_1^2/2u_0^3](du_0/d\tau)^2.$$

These three sets of equations give the multiple scales initial value problem to the orders indicated and they should permit the solution to the order ϵ to be found. We can only present the solution u_0 here, however.

This zero-order problem contains the only nonlinear differential equation among the three given above. Aside from the normalization and the lack of a forcing function, it strongly resembles the autonomous equation dealt with in the cutoff calculations above. As we shall see, the above rather small changes can make a significant difference in the nature of the solutions that we shall obtain.

The Zero-Order Solution

Analytical Background

For convenience we shall drop the subscript zero temporarily, and write

$$u(d^2u/d\tau^2) + (3/2)(du/d\tau)^2 = \gamma/[(1+Q)^5u^3] - 1/(1+Q)^3u,$$

$u(0) = 1,$ (27)

and

$(du/d\tau)_{(\tau=0)} = 0.$

It is well known that if we put $du/d\tau = v$ we can replace the second order differential equation in Eqs. (27) with a coupled pair of first-order equations. These read

$v = du/d\tau$

and

$$d(u^3v^2)/du = [2\gamma/(1+Q)^5]/u - u/(1+Q)^3.$$

The second of these equations has the first integral

$$u^3v^2 = (2\gamma\,\ell n\,u)/(1+Q)^5 - u^2/(1+Q)^3 + [A + (1+Q)^{-3}],$$

in which the quantity, $[A + (1+Q)^{-3}]$, is the constant of integration. We can rewrite this to read

$$u^3v^2 = (2\gamma\,\ell n\,u)/(1+Q)^5 - (u^2-1)/(1+Q)^3 + A, \qquad (28)$$

and the condition, $u(0) = 1$, is satisfied. Now, the left-hand side of this first integral is proportional to the kinetic energy of the bubble motion. The right-hand side is proportional to the potential energy, $-V$, of the bubble and the constant A permits one to adjust the level of V. On the other hand if the condition, $(du/d\tau)_{(\tau=0)} = 0$, is also satisfied we must set $A = 0$. Moreover, had we replaced the forcing function, $f(\tau; K)/(1+Q)^2$, in Eq. (22a) with a step function, $F_c/(1+Q)^2$, we would add the term, $2[F_c(u^3-1)]/[3(1+Q)^2]$, to the right-hand side of Eq. (28) above.

Phase-Plane Analysis

Next we could plot V(u), including the added term, as shown in Fig. 9a. From its level lines and Eq. (28), including the F_c term, we can find the corresponding phase-plane trajectories as shown in Fig. 9b. This figure is a very familiar illustration of the global nature of the well known autonomous solution and it shows where the vortex and saddle points are to be found in the phase plane. These can be located precisely with the help of Liapunov's method or directly from the potential energy curve. The limiting velocity, $\sqrt{[2F_c/(1+Q)^2]}$, shown in Fig. 9 is due to the step-function forcing function and we see that it is naught in the present zero-order solution because $F_c = 0$.

While the foregoing discussion reviews knowledge regarding general features of the zero-order solution, it remains for us to narrow our view and to examine the problem at hand. This we do by considering the basic solution, Eq. (28), with $A = F_c = 0$. Then both initial conditions are satisfied and this particular form of the differential equation (28) enables us to study the phase-plane trajectories and

the position of the singularities on the u axis as the parameter Q varies over the range of interest. Figure (10) shows the results of this investigation for one value of the dissolved air-content parameter, $\gamma = 1.4$ for saturated water. Now the saddle point has been lost and all trajectories originate at $u = 1$ by design.

The dotted curve in the upper potential-

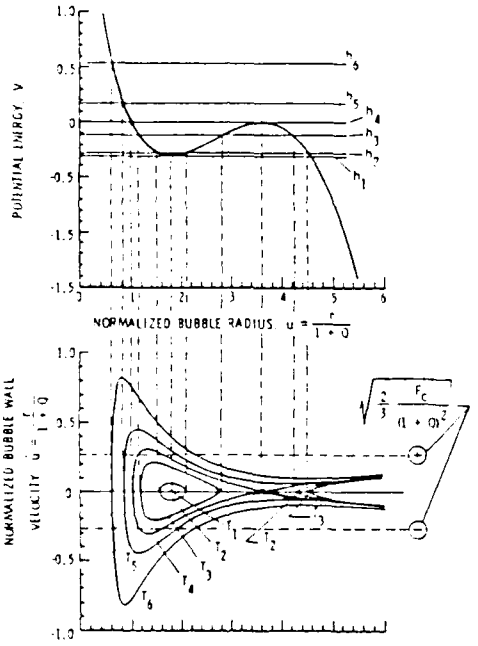

Figure 9.- Phase plane and level lines for a step-forced isothermal cavitation bubble.

(a) Potential curve and level lines.

(b) Phase-plane trajectories.

energy plot corresponds to the case where the trajectory and the vortex are contained at the origin in the phase plane. The motion is then defined by the solution $u(\tau) = 1$ and $v(\tau) = 0$. This null-motion finding overlooks the fact noted previously that the initial velocity is actually an extremely small positive number. But since this model of the oscillations has no zero-order energy source the resulting oscillations are well represented by the trivial solution just given.

The important feature is that this "critical" case represents the condition of demarcation between two physically distinct motions. Trajectories on the left represent

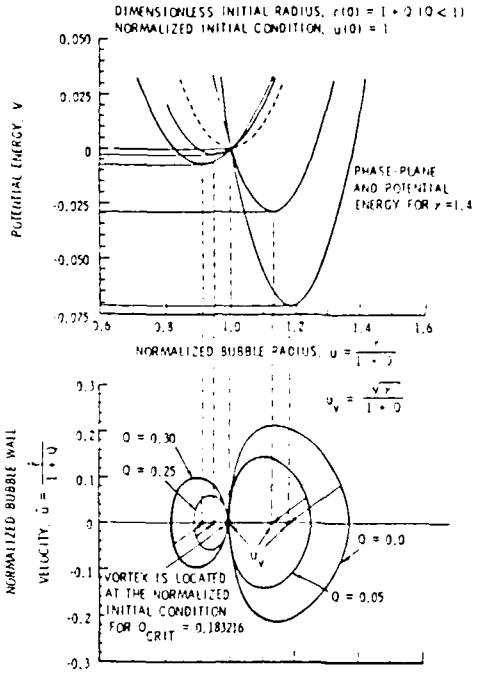

Figure 10.- Phase plane and level lines for the zero-order analysis.

(a) Potential curves and level lines for various values of Q and one dissolved air content.

(b) Phase-plane trajectories, originating at $u = 1$, for various Q values.

small scale flaccid air bubble oscillations whereas those on the right are somewhat larger amplitude oscillations involving vaporous growth, although the gas in the bubble is also important in the motion. The way in which the phase-plane singularities move along the real axis and the size of the trajectories as the value of Q changes from 0.0 to 0.3 is clearly illustrated in Fig. 10. Moreover, the potential energy minimum is found at $u_v = (\sqrt{\gamma})/(1 + Q)$, which defines analytically the vortex point locations. For any air content we can write $Q_{crit} = (\sqrt{\gamma}) - 1$. If $Q_{crit} = 0$, then $(\sqrt{\gamma}) = 1$ and this indicates the lowest value of dissolved air content for positive values of Q. Referring to Eq. (18a) which defines Q, we see that this limit would correspond to $V_0 = 0$ or to $K = 0$, because it is physically unrealistic for the surface tension to be infinite.

Of course, all of these free oscillations are of high frequency. It is of interest to find out

how many cycles of free oscillation might be found during the time of rise for one of the forcing functions of Fig. 8. This rise time is measured in units of laboratory time. Some calculations have been made to answer this question and these will be discussed later. For now we may say that during a typical bubble time interval between F(0; K) = 0 and F(τ; K) = $F_{|max}$ the number of vaporous oscillations is measured in multiples of ten. It may be pure coincidence, but the amplitudes of oscillation indicated here and those illustrated in Fig. 2 appear to be about the same and so the frequencies also should be comparable. It should be said however, that the results found here show a weak dependence on K and V_0 and these results, being of order zero in ε, are independent of the forcing function. Therefore, the apparent consistency between the present and the older results is very encouraging. Those older results also suggest how the influence of the forcing function grows to produce a large vaporous growth which overwhelms the small scale free oscillations considered here. Further exploration of these additional aspects of the process depend on the first-order solution which remains a topic for future research.

Zero-Order Analytical Solution

Using the fact that v = du/dτ and solving for v in Eq. (26), we can write Eq. (28) as

$$(du/d\tau)^2 = [(2\gamma \ln u)/(1 + Q)^5 - (u^2 - 1)/(1 + Q)^3]/u^3.$$

The bubble time, τ, is then given as the quadrature,

$$\tau = \int_1^u x^2 dx/\sqrt{(2\gamma x \ln x)/(1+Q)^5 - (x^3 - x)/(1 + \quad)^3}. \quad (29)$$

Generally, one evaluates this integral numerically. It is possible to obtain a reasonably accurate approximate solution by fitting the function u ln u with a cubic polynomial, $au^3 + bu^2 + cu + d$. The coefficients are a = -0.050304, b = 0.578693, c = - 0.001871, & d = - 0.526519. Then the radicand above also becomes a cubic, $Ax^3 + Bx^2 + Cx + D$, having coefficients:
A = [2γa/(1 + Q)^5] - [1/(1 + Q)^3], B = 2γb/(1 + Q)^5, C = 2γc/(1 + Q)^5 + [1/(1 + Q)^3], & D = [2γd/(1 + Q)^5].

As a rule this cubic can be factored with the help of Tartaglia's method. But first the radicand should be rewritten as A [$x^3 + px^2 + qx + r$]. Then if we put $u_v = \sqrt{\gamma}/(1+Q)$ we have
p = $2bu_v^2/(2au_v^2 - 1)$, q = $(2cu_v^2 + 1)/(2au_v^2 - 1)$ and r = $2du_v^2/(2au_v^2 - 1)$.

Let the three real roots of this modified cubic be x_1, x_2, and x_3, and suppose that they are ordered with respect to the upper limit of integration to read, $x_1 < x_2 \leq u < x_3$. The usual laborious factorization can be shortened in this case by observing that the rewritten cubic always has one root equal to unity. Thus when one divides the cubic, $x^3 + px^2 + qx + r$, by the factor, x - 1, the remainder turns out to be $2u_v^2(a + b + c + d)/(2au_v^2 - 1)$. Then when the numerical values of a,b,c and d are summed as indicated, one finds this sum equal to -0.000001 and he can consider this result to be zero for all values of u_v, within the accuracy of these four coefficients. Consequently, we need only factor the quadratic,

$$x^2 + x(2au_v^2 - 1 + 2bu_v^2)/(2au_v^2 - 1) + 2u_v^2(a + b + c)/(2au_v^2 - 1).$$

These factors are

$$[(1.0568u_v^2 - 1)/2(1 + 0.100608u_v^2)]\ \{\ 1 \pm \sqrt{Z}\ \},$$

where

$$Z = 1 + [4.212144u_v^2(1 + 0.100608u_v^2)/(1.0568u_v^2 - 1)^2].$$

These roots were also found numerically for the specific example of u_v = 1.1832, corresponding to γ = 1.4 and Q = 0.0. The three roots are x_1 = - 0.9459, x_2 = 1.0 and x_3 = 1.3662. Comparison of these with the range of integration in Eq. (29) justifies the above ordering of the roots with respect to the value u, in this case at least. Moreover, except for x_1, the roots depend on u_v, that is $x_i = x_i(u_v)$. Also u_v will be recognized as the parameter governing the location of the singularities in the phase plane. The root at u = x_2 = 1.0 is seen to be the initial point in the phase plane. The dependence of the other roots on u_v, permits one to distinguish between the families of trajectories to the right or to the left of the initial point in Fig. 10 above. The junior author has investigated this last matter fully in his thesis.

Consequently Eq. (29) can be rewritten using roots x_1, x_2, and x_3, as

$$\tau = \sqrt{(1+Q)^3/(2au_v^{2}+1)} \int_1^u x^2 dx/G(x) \,, \quad \text{where} \quad G(x) = \sqrt{(x-x_1)(x-x_2)(x_3-x)} \qquad (29a)$$

and the value of a is given above . With the help of Byrd and Friedman[7], Eq. (29a) can be expressed in terms of incomplete elliptic integrals of the first, second and third kinds and a product of Jacobian elliptic functions. We are not aware of any method for inverting that complicated result so that it will have the form $u = f(\tau)$. Therefore we did repeated numerical integrations and varied the quantity $u_v = \sqrt{\gamma}/(1+Q)$ over the range indicated in the phase plane analysis above and selected an appropriate intermediate value of $(1+Q)^{3/2}$ with the result illustrated in Fig. 11.

The relation shown in Fig. 11 was fit with an approximate analytical result, which is accurate at the origin and at all maximum radii, r_m. It is a simple expression and in the worst case it offers about 5% or 13% accuracy between these limits depending on whether one uses u or (u - 1) in the calculation of relative error. This simple aproximation has the form

$$u = A + B\cos(\psi) + C\cos(2\psi). \qquad (30)$$

The angle $\psi = \psi(u_v,\tau)$ and the coefficients, A,B and C, which also depend on u_v contain all of the complexity. The degree of success achieved with this formula is shown in the comparison in Fig. 12. Note that the ordinate in Fig. 12 has a suppressed zero so that the illustration emphasizes differences between this approximation, shown as dashed curves, and solid-line numerical results from Eq. (29a). Equation (30) is an important first step toward achieving the desired precise result for the zero-order solution. It suggests that over the parameter range of interest here, a more refined representation of $u_0(\tau, u_v)$ can now be found. This final result and other details not presented above are given in the junior author's thesis.

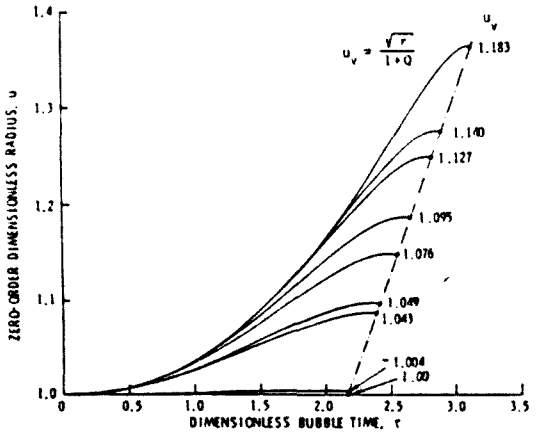

Figure 11.- Numerical results for zero-order isothermal cavitation bubble growth on a hemispherical headform.

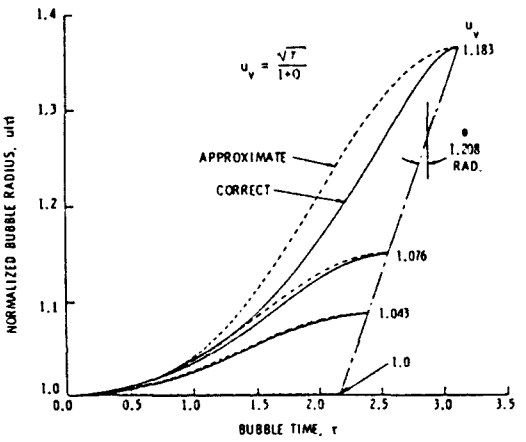

Figure 12.- Comparison of numerical results from Fig. 11 with the fitting function of Eq. (30).

Conclusions:

Perhaps the chief point needing emphasis with regard to our review of the so-called asymptotic bubble-ring inception theory is that its postulates do not allow for nuclei recirculation within the laminar bubble after they have been created by the visible bubble-ring cloudlets in the transition zone. That is to say, we are not concerned with desinence. Our interest is in inception only. In this latter situation there will be no ring of cloudlets and we must assume that the only nuclei source is from the free stream. The apparent good agreement shown in Fig. 3 leaves us with the hope that the basic assumptions of the theory are close to the truth.

The ability of the cavitation-cutoff theory, as outlined above, at least to show

correct trends reinforces the hope that our basic postulates are correct. The question is: Will a more refined calculation as initiated here improve the ability of the theory to predict cavitation cutoff speeds? At present we can not say. But more comprehensive experimental cutoff data would be of great value for testing this aspect of the theory .

Turning to the multiple scale calculations, we can say that an approximate zeroth-order solution is now in hand. It remains to find the first-order solution and to put these two parts of the solution into a form which is ready for more refined scaling and cutoff calculations. We hope that research aimed at completing this work can be carried out soon.

Acknowledgment

This work was sponsored by the Naval Sea Systems Command, by Dr. Thomas E. Peirce, Code NSEA 63R31 and by the NSEA General Hydrodynamics Research program, under Mr. V. J. Monacella, The David Taylor Naval Ship Research and Development Center, Code 1504. The opinions expressed herein do not reflect any policy of the U.S. Navy.

References:

1. Plesset, M. S., "Dynamics of Cavitation Bubbles," *Trans. ASME,* Vol. 71, *Journal of Applied Mechanics,* Vol. 16, 1949, p. 277.

2. Gates, E. M., and Bacon,J., "A Note on the Determination of Cavitation Nuclei Distributions by Holography," *Journal of Ship Research,* Vol. 22, No. 1, March 1978, pp. 29 - 31.

3. Arakeri, V. H., "Viscous effects in Inception and Development of Cavitation on Axi-Symmetric Bodies," Ph.D. Thesis, California Institute of Technology, 1973 (Also released as Report No. 3183.1, Division of Engineering and Applied Science, California Institute of Technology, 1973.)

4. van der Meulen, J.H.J., "A Holographic Study of Cavitation of Axisymmetric Bodies and the Influence of Polymer Additives," Ph.D. Thesis, Enschede, 1979.

5. Holl, J. W. and Carroll, J. A., "Observations of the Various Types of Limited Cavitation on Axsymmetric Bodies," Proceedings of the International Symposium on Cavitation Inception, The ASME, New York, December 1979, p. 87.

6. Parkin, B. R., "A Theory for Cavitation Inception in a Flow Having Laminar Separation," Technical Memorandum file No. TM 79-198, Applied Research Laboratory, The Pennsylvania State University, P.O. Box 30, State College, PA. 16804. See also *Trans. ASME, Jour. of Fluids Engineering* , Vol. 103, No.4, Dec. 1981, p 543 and p. 577; also Vol. 104, No. 1, March 1982, p. 115.

7. Byrd, P. F. and Friedman, M. D. *Handbook of Elliptic Integrals for Engineers and Physicists,* Springer Verlag, Berlin, 1954.

DISTRIBUTION LIST FOR UNCLASSIFIED TECHNICAL MEMORANDUM 86-121, BY B. R. PARKIN AND B. B. BAKER, DATED 30 JULY 1986

Defense Technical Information Center
5010 Duke Street
Cameron Station
Alexandria, VA 22314
(Copies 1 through 6)

Commanding Officer
David W. Taylor Naval Ship Research & Development Ctr.
Department of the Navy
Bethesda, MD 20084
Attention: M. Tod Hinkel [Code 1504]
(Copies 7 through 12)

Naval Research Laboratory
Marine Technical Division
Department of the Navy
Washington, DC 20390
Attention: R. J. Hansen
(Copy No. 13)

Commander
Naval Sea Systems Command
Department of the Navy
Washington, DC 20362
Attention: T. E. Peirce [Code NSEA 63R-31]
(Copy No. 14)

General Electric Company
VA 95 Business Park
8080 Grainger Court
Springfield, VA 22153
Attention: B. B. Baker
(Copies 15 and 16)

Director
Applied Research Laboratory
The Pennsylvania State University
Post Office Box 30
State College, PA 16804
Attention: M. L. Billet
(Copy No. 17)

Director
Applied Research Laboratory
The Pennsylvania State University
Post Office Box 30
State College, PA 16804
Attention: L. R. Hettche
(Copy No. 18)

Director
Applied Research Laboratory
The Pennsylvania State University
Post Office Box 30
State College, PA 16804
Attention: J. W. Holl
(Copy No. 19)

Director
Applied Research Laboratory
The Pennsylvania State University
Post Office Box 30
State College, PA 16804
Attention: B. R. Parkin
(Copy No. 20)

Director
Applied Research Laboratory
The Pennsylvania State University
Post Office Box 30
State College, PA 16804
Attention: GTWT Files
(Copy No. 21)

Director
Applied Research Laboratory
The Pennsylvania State University
Post Office Box 30
State College, PA 16804
Attention: ARL/PSU Files
(Copy No. 22)

END

DTIC

9-86